Journal of Sol-Gel Science and Technology (2018) 87:442–454
https://doi.org/10.1007/s10971-018-4723-x

ORIGINAL PAPER: SOL-GEL AND HYBRID MATERIALS WITH SURFACE MODIFICATION FOR APPLICATIONS

Preparation and application of phosphinic acid functionalized nanosilica for the effective removal of mercury (II) in aqueous solutions

Chao Xiong[1] · Shixing Wang[1,2] · Libo Zhang[1,2] · Ying Li[1] · Chandrasekar Srinivasakannan[3] · Jinhui Peng[1,2]

Received: 22 February 2018 / Accepted: 6 June 2018 / Published online: 16 June 2018

Abstract
A novel adsorbent was synthesized by functionalizing nanosilica with phosphinic acid groups for the removal of mercury ions from aqueous solutions. The synthesized absorbent was characterized by Fourier transform infrared spectroscopy (FT-IR), X-ray photoelectron spectroscopy (XPS), transmission electron microscope (TEM) and thermogravimetric analysis (TGA). Meanwhile, the effects of initial pH, contact time and initial mercury ions concentration on the removal of mercury ions from aqueous solutions were investigated by batch adsorption experiments. The results showed that the removal rate reached 99.11% and the maximum adsorption capacity was up to 274.32 mg/g at pH 2 and the equilibrium time of adsorption was about 1 h. The absorbent presented good selectivity for mercury ions among Zn(II), Ni(II), Mn(II) and Ge (IIII). Moreover, the obtained adsorbent has good reusability and the absorbability decreased only from 98.76 to 94.75% after five cycles. Besides, the adsorption isotherms fitted well to the Langmuir isotherm model and adsorption kinetics followed the pseudo-second-order model. The removal mechanism of mercury via phosphinic acid-functionalized silica nanoparticles was chelation interaction. All the experimental data indicated that the phosphinic acid-functionalized silica nanoparticles are very promising in removal of mercury ions from aqueous solutions.

✉ Shixing Wang
wsxkm@sina.com

✉ Libo Zhang
zhanglibopaper@126.com

[1] Faculty of Metallurgical and Energy Engineering, Kunming University of Science and Technology, Kunming, Yunnan 650093, PR China

[2] State Key Laboratory of Complex Nonferrous Metal Resources Clean Utilization, Kunming University of Science and Technology, Kunming, Yunnan 650093, PR China

[3] Department of Chemical Engineering, Khalifa University of Science and Technology, Abu Dhabi, United Arab Emirates

Graphical Abstract

A novel adsorbent was synthesized by functionalizing nanosilica with phosphinic acid groups for the removal of mercury ions from aqueous solutions. The adsorbent presented good selectivity and reusability. The removal mechanism is chelation interaction between mercury ions and PA-SNPs.

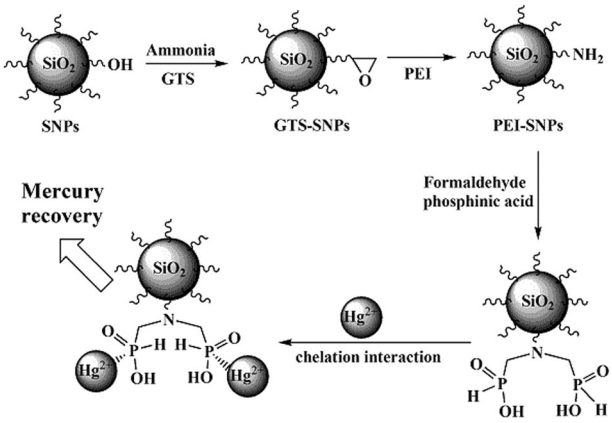

Highlights

- A new adsorbent was prepared via modifying nanosilica with phosphinic acid groups
- The adsorbent exhibits an excellent selectivity for mercury ions
- The adsorbent showed a maximum adsorption capacity of 274.32 mg/g for mercury ions under pH 2
- The removal mechanism was chelation interaction.

Keywords Adsorbent · Nanosilica · Mercury ions · Removal · Mechanism · Reusability

1 Introduction

Over the past several years, water pollution has been a global problem with rapid industrial development [1, 2]. Mercury pollution is one of the most severe problems because of its high toxicity and non-biocompatibility. Various industrial activities have discharged a large amount of mercury into wastewater, such as batteries, metal plating, mining, paint manufacturing and photographic industry [3]. Besides, mercury enters the food chain through various pathways during the circulation of water, leading to many diseases, such as Alzheimer's disease, loss of vision, deafness, mental disorder, congenital malformation of children and memory impairment [4–6]. Therefore, it is a very important to remove mercury ions from aqueous solutions.

Generally, the removal methods of mercury ions from aqueous solutions include chemical precipitation, ion exchange, liquid extraction, photo reduction, coagulation, membrane filtration, solvent extraction and adsorption [7–9]. Among these removal methods, adsorption was considered as a promising method to remove mercury ions from aqueous solutions because of its high efficiency, good reutilization, low cost and environmental friendliness [10, 11]. Many adsorbents were reported in the literatures, such as rice straw, activated carbon, carbon nanotube, polystyrene, chitosan, silica gel, zeolite, coconut husk, cellulose, polymer materials, nanosilica, and so on [12–15]. Nanosilica is widely concerned because of their unique physical and chemical properties, such as low cost, large specific surface area and easy regeneration [16]. Besides, nanosilica is easy to be functionalized by chemical or physical methods than other adsorbents [17]. In general, the adsorption capacity of adsorbent is mainly determined by surface area and functional group density. The functionalized nanosilica has the intrinsic characteristics of nanosilica and the inherent characteristic of the functional group [18]. So, surface functionalized nanosilica is a promising sorbents for metal ions removal.

In recent years, hypophosphate has attracted great interests because phosphorus compounds with P–O or P=O groups are very effective ligands for heavy metal ions based on Lewis acid base theory [19]. Wang, et al. reported that phosphinic acid groups coordinated with a variety of transition-metal ions [20]. Therefore, many phosphated materials are used for metal ion removal. The phosphate nanocelluloses selectively adsorbed Ag^{+}, Cu^{2+}, and Fe^{3+} from industrial effluents [21]. The phosphorylated nanofibrils improved the sorption rate and capacity of copper from contaminated water [22]. Therefore, it is a potential solution for water treatment to modify phosphate groups on the surface of materials.

In this article, a novel adsorbent was synthesized by modifying nanosilica with phosphinic acid for mercury ions removal from aqueous solutions. This adsorbent was characterized by Fourier transform infrared spectroscopy (FT-IR), X-ray photoelectron spectroscopy (XPS), transmission electron microscope (TEM) and thermogravimetric analysis (TGA). Simultaneously, the effect of the solution pH, initial mercury ions concentration, contact time and coexisting ions was systematically investigated. Besides, selectivity, reusability (five cycles), adsorption mechanism, adsorption isotherms (Langmuir and Freundlich) and kinetics (Pseudo-first-order kinetic and Pseudo-second-order kinetic) were also studied.

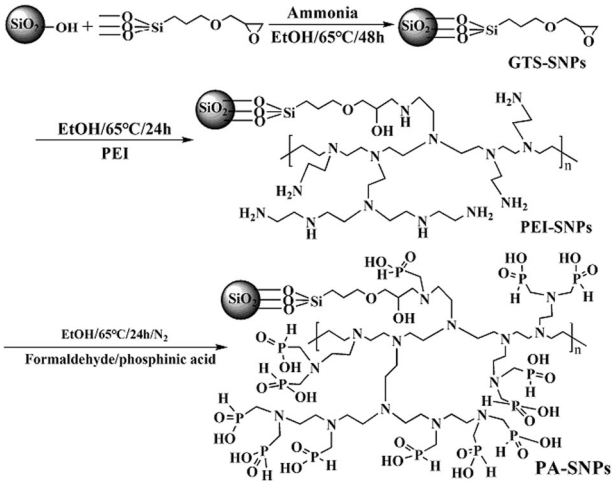

Scheme 1 The synthesis process of PA-SNPs

2 Materials and methods

2.1 Materials

Polyethyleneimine (PEI), (3-glycidyloxypropyl)trimethoxysilane and nanosilica (SNPs, Hydrophilic-380, 99.8%) were purchased from the Aladdin Chemistry Co. Ltd., Shanghai, china. Ammonia (25%), phosphinic acid, thiourea (99%), ethanol (99.8%) and formaldehyde were purchased from Tianjin Chemical Reagent Co. Ltd. HNO_3 (67%) and NaOH (99%) were purchased from Nanjing Chemical Reagent Co. Ltd. $Hg(NO_3)_2$, $Zn(NO_3)_2$, $Ni(NO_3)_2$, $Mn(NO_3)_2$, and $Ge(NO_3)_4$ were purchased from National Nonferrous Metals Research Institute, Peking, China. All of the chemical reagents were analytical grade and without further treatment. The effects of coexisting ions on mercury adsorption were detected by adding the salt of the coexistence ion into the mercury solutions. The pH value of solutions was adjusted by 0.1 mol/L HNO_3 and 0.1 mol/L NaOH solutions.

2.2 Preparation of phosphinic acid functionalized nanosilica

The preparation process of the phosphinic acid functionalized nanosilica was presented in Scheme 1. Firstly, the mixture of 3-glycidoxypropyltrimethoxysilane (10 mL), SNPs (5 g), ethanol (100 mL) and ammonia (2 mL) was stirred and refluxed at 65 °C for 48 h. After centrifugation, the solid was washed with ethanol five times, and dried at 60 °C for 12 h in vacuum drying oven. The obtained sample was denoted as GTS-SNPs. Secondly, the mixture of GTS-SNPs (4.5 g), PEI (100 mg/mL) and ethanol (50 mL) was stirred and refluxed at 65 °C for 24 h. After centrifuged, the solid was washed with distilled water and then dried at 60 °C for 12 h. The obtained sample was denoted as PEI-SNPs. Finally, the mixture of PEI-SNPs (5 g), phosphinic acid (15 mL), formaldehyde (40%, 15 mL) and ethanol (30 mL) was stirred and refluxed at 65 °C for 24 h under N_2. After centrifuged, the solid was washed with distilled water and dried at 60 °C for 12 h. The obtained white powder was denoted as PA-SNPs.

2.3 Characterization

Fourier transform infrared spectroscopy (FT-IR, Nicolet iS50, USA) was used to characterize the surface functional groups of adsorbents. Thermogravimetric analysis (TGA) were measured by PerkinElmer TGA-8000 (US) thermogravimetric analyzer at a heating rate of 10 °C/min. X-ray photoelectron spectroscopy (XPS, Physical Electronics, Inc., Chanhassen, MN, 200 W Mg radiations, USA) was used to investigate the surface chemical states of samples. Transmission electron microscope (TEM, JEM-3200) was used to evaluate the morphology of the nanoparticles. Inductively coupled plasma optical emission spectrometer (ICP-OES, Leeman prodigy 7, America) was used to detect the concentration of metal ions.

2.4 Mercury adsorption experiments

The adsorption experiments of mercury ion were carried out by adding 20 mg PA-SNPs into a series of centrifuge tube containing mercury ion solution (10 mL) with desired initial concentration and pH. The mixtures were shaken in a ZD-85 thermostat oscillator at 25 °C with constant rate of 300 rpm for a given time. After centrifuged at 8000 rpm for 15 min, the concentration of mercury ion was determined by ICP-OES.

The effects of pH, initial mercury ion concentration and contact time were investigated. The desired pH (ranging from 1.0 to 6.0) was adjusted by HNO_3 (0.1 mol/L) and

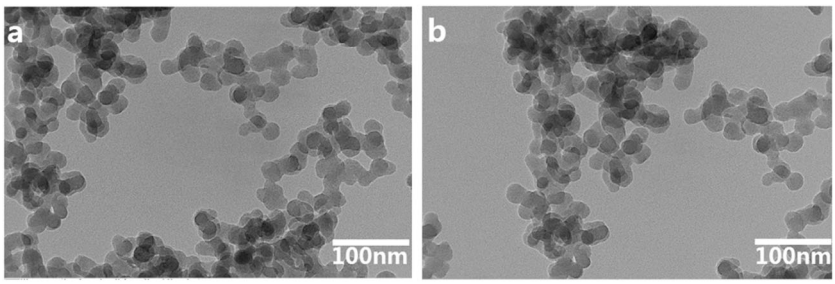

Fig. 1 TEM images of SNPs and PA-SNPs

NaOH (0.1 mol/L) solutions. The selective separation of mercury ion from coexisting ions (Ge(IIII), Ni(II), Zn(II) and Mn(II)) was carried out when all ions concentrations were 100 mg/L. The concentration of mercury ion was 100 mg/L for kinetic study and 100–800 mg/L for isotherm study. In addition, the contact time of mercury ion with PA-SNPs was 5–720 min. The equilibrium adsorption capacity (q, mg/g) and removal rate (R, %) of mercury ion by PA-SNPs were calculated by following equation [23, 24].

$$q = (C_0 - C_e)\frac{V}{m} \quad (1)$$

$$R = \left(1 - \frac{C_e}{C_0}\right) \times 100\% \quad (2)$$

Where C_0 (mg/L) and C_t (mg/L) are the initial and final concentration of mercury ion, respectively. V (mL) represents the volume of the mercury ion solution and m (mg) represents the mass of PA-SNPs sorbent.

2.5 Mercury desorption

The desorbing agent is made up of nitric acid (3 mol/L) and thiourea (1.5 mol/L). In order to better examine the reusability of PA-SNPs, the mixture of PA-SNPs (80 mg) and mercury ions solution (40 mL, 100 mg/L) was oscillated in thermostatic oscillator for 2 h at 25 °C. The solid was filtrated and the solution was retained for detection. The remaining solid was treated with the desorbing agent for 24 h. Then, the solid was washed with distilled water for five times and conduct the second round of adsorption. The above procedures were repeated for five times.

3 Results and discussion

3.1 Characterization of the phosphinic acid functionalized nanosilica

Figure 1 showed the TEM image of SNPs and PA-SNPs. The particles sizes of SNPs and PA-SNPs were 12.5 ± 5.0 nm. There was no significant size change between SNPs and PA-SNPs.

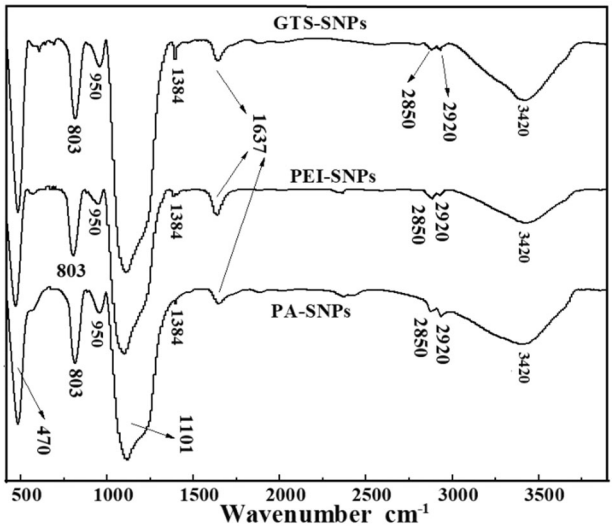

Fig. 2 FT-IR spectra of GTS-SNPs, PEI-SNPs, and PA-SNPs

Figure 2 has given FT-IR spectra of GTS-SNPs, PEI-SNPs and PA-SNPs. The peaks at 470, 803, and 1101 cm^{-1} were assigned to Si–O–Si bending vibration, symmetric stretching and stretching vibration, respectively [25–27]. The peak at 950 cm^{-1} was attributed to Si–OH group vibration [28]. For the effects of adsorbed water and silanol groups, the peaks at 3420 and 1637 cm^{-1} were attributed to O–H stretching vibration and deformation vibration, respectively. In the spectra of GTS-SNPs, the peaks at 2920 and 2850 cm^{-1} were attributed to the C-H stretching vibration, indicating that organic silane was grafted onto the surface of silica nanoparticles successfully. In the spectrum of PEI-SNPs, The band at 1384 cm^{-1} was attributed to the $–NH_2$ and –NH bending vibration. For PA-SNPs, the peaks at 1384 cm^{-1} for the $–NH_2$ and –NH bending vibration were disappeared, due to the reaction between phosphonic acid groups and the $–NH_2$ and –NH [19]. Besides, the peaks for phosphinic acid groups (including P=O bond adsorption peak at 1185 cm^{-1}, PO_2 stretching vibrations at 1054 and 1185 cm^{-1}) were no obvious indication in FT-IR spectra of PA-SNPs because they are overlapped by the broad bond between 1101 cm^{-1}[19, 24, 29].

Figure 3 presented the TGA analysis of SNPs, GTS-SNPs, PEI-SNPs and PA-SNPs. The mass loss of SNPs, GTS-SNPs, PEI-SNPs and PA-SNPs were 6.1, 8.5, 12.4, and 15.7%, respectively. The mass loss was due to the decomposition of organic matter and evaporation of water. The calculated amounts of 3-glycidoxypropyltrimethoxysilane, polyethyleneimine and phosphinic acid on the surface of SNPs were 2.66, 3.39, and 6.44%, respectively.

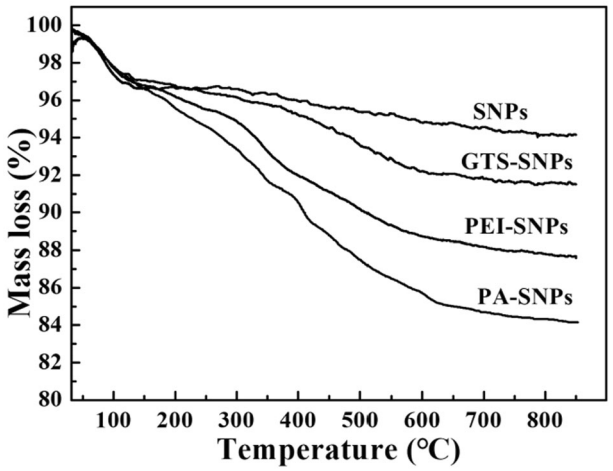

Fig. 3 TGA analysis of SNPs, GTS-SNPs, PEI-SNPs, and PA-SNPs

Figure 4 (a) showed the wide-scan spectra of GTS-SNPs, PEI-SNPs and PA-SNPs. The nitrogen peak around 400 eV was appeared after the GTS-SNPs were modified by PEI, indicating PEI groups were grafted onto the surface of silica nanoparticles successfully. A signal spectra at 168.2 eV presented in XPS wide-scan spectra of PA-SNPs was attributed to P2p, arising from the phosphinic acid group. This indicated phosphinic acid groups were grafted onto the surface of silica nanoparticles successfully. The C1s spectra of GTS-SNPs, PEI-SNPs and PA-SNPs were showed in Figs. 4b–d. Two peaks at 284.6 and 285.8 eV (Fig. 4b) in the C1s spectra of GTS-SNPs were corresponded to C-C (C-H) and C-O bonds, respectively. The new peak at 286.4 eV was corresponded to C-N bond (Fig. 4c). After modification by phosphinic acid, the new peak at 285.4 eV was attributed to the C-O(PO) of the phosphinic acid groups (Fig. 4d). Therefore, The XPS analyses further demonstrated that the phosphinic acid functionalized nanosilica was successfully synthesized. Besides, the isotherm linear of PA-SNPs was shown in Fig. 5. The BET results showed that the specific surface area, pore volume and pore size of

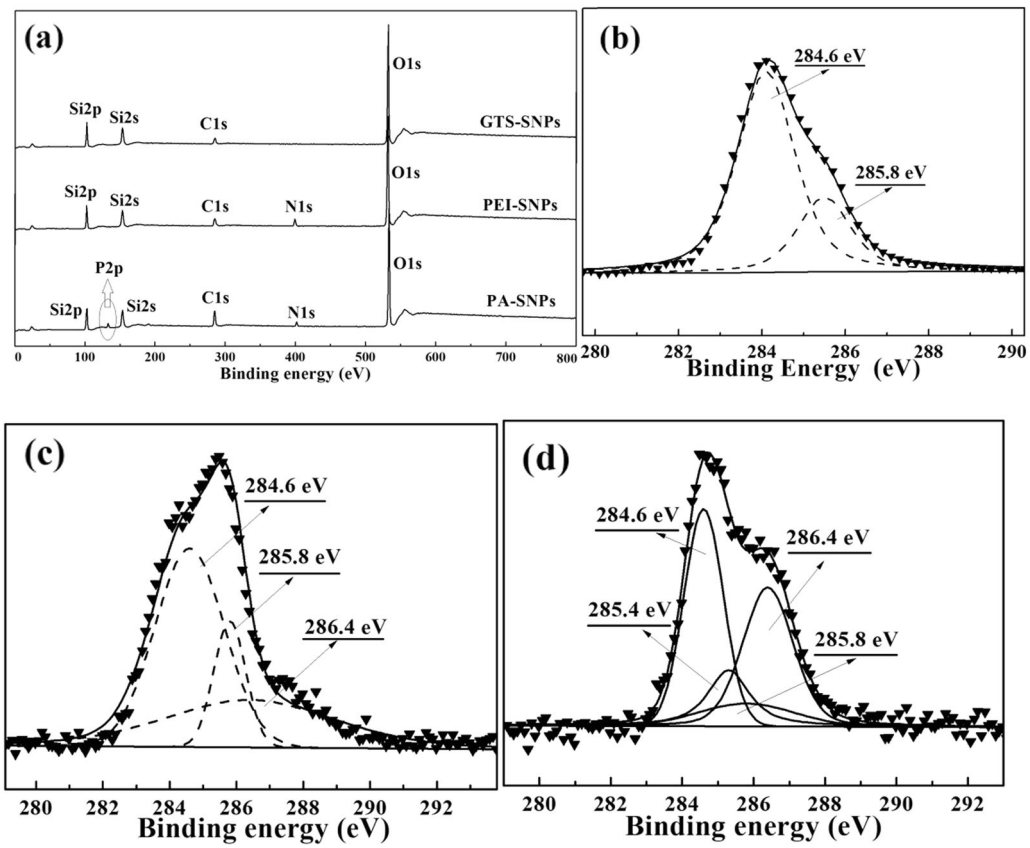

Fig. 4 XPS wide-scan spectra and C1s spectra of GTS-SNPs, PEI-SNPs, and PA-SNPs

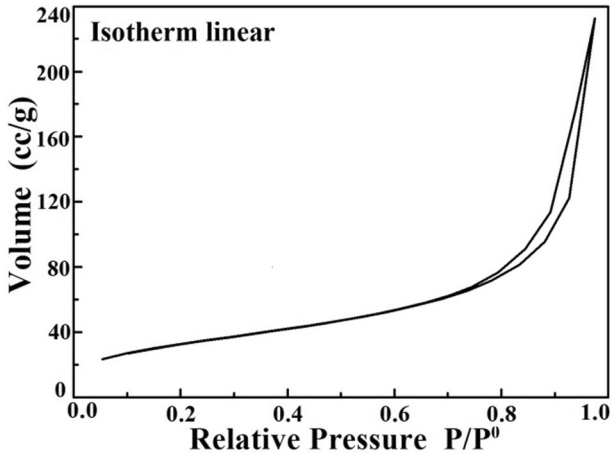

Fig. 5 The isotherm linear of BET surface area

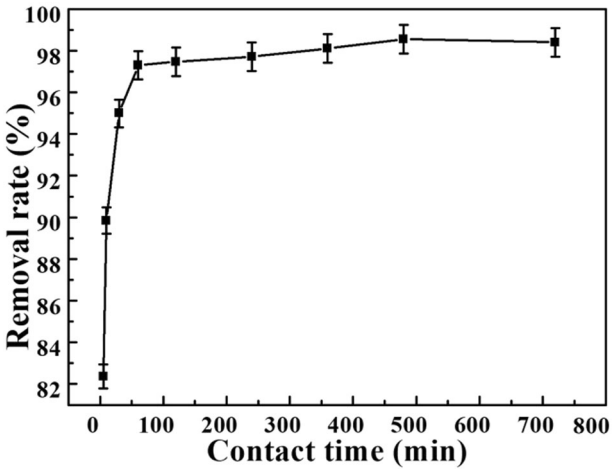

Fig. 7 Effect of contact time on the removal rate of Hg(II)

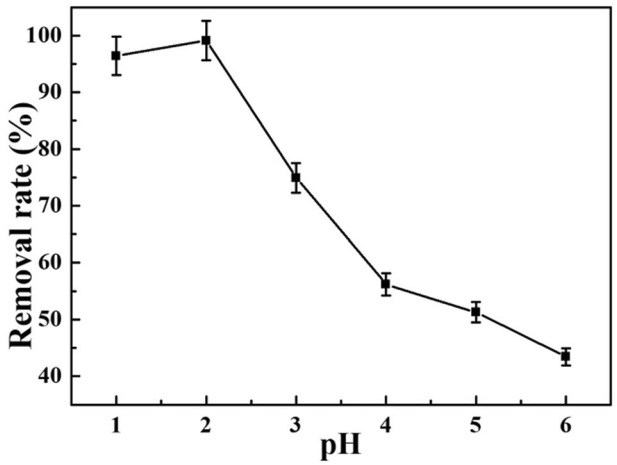

Fig. 6 Effect of initial pH on Hg(II) adsorption

PA-SNPs were 116.459 m^2/g, 0.328 cm^3/g, and 3.253 nm, respectively.

3.2 Adsorption performance

3.2.1 Effect of pH

The pH of the solution is a crucial factor in the adsorption process. Because pH affects the surface properties of adsorbents in terms of dissociation of functional groups and surface charge. In order to prevent the hydrolysis of Hg^{2+} when pH value is greater than 6, the adsorption experiments of mercury ion were carried out in the pH range of 1.0 to 6.0. PA-SNPs (20 mg) and mercury ion solution (10 mL, 100 mg/L) were stirred in a ZD-85 thermostat oscillator at 25 °C for 12 h. Figure 6 showed the effect of pH on the removal rate of mercury ions. The result showed that maximum removal rate of mercury ion was obtained at pH 2. At low pH (<2.0), the removal rate of mercury ions by PA-SNPs increases with the increase of pH. Because H^+ will neutralize the surface charge, the H_3O^+ ions was preferably adsorbed on PA-SNPs and prevented the sorption of mercury ions at low pH [19, 30]. At higher pH, the concentration of H^+ in solution decrease with the increase of pH. Moreover, Hg^{2+} converted into the metal hydroxide species, such as $Hg(OH)_2$ or $Hg(OH)^+$. Therefore, the removal rate of mercury ions by PA-SNPs decreases with the increase of pH from 2 to 6. So, the following experiments were carried out at pH 2.

3.2.2 Effect of contact time on the removal rate and adsorption kinetics

20 mg of PA-SNPs was added into 10 mL of the mercury solution with the concentration of 100 mg/L at pH 2. The influence of the contact time on removal rate of Hg^{2+} was shown in Fig. 7. It can be found that the removal rate was extremely rapid within the initial few minutes and reached the adsorption equilibrium at 60 min. In the initial stage, the fast adsorption should attribute to the small mass transfer resistance, plenty of functional groups and large specific surface area on the PA-SNPs [31, 32]. In the equilibrium stage, the adsorption was slowed down as the active sites of PA-SNPs were filled up.

In order to evaluate the kinetic mechanism, two models were employed to interpret the experimental data. The pseudo-first-order and pseudo-second-order models are represented as Eq. (3) and Eq. (4) [33, 34]:

$$\ln(q_e - q_t) = \ln q_e - k_1 t \quad (3)$$

$$\frac{t}{q_t} = \frac{1}{k_2 q_e^2} + \frac{t}{q_e} \quad (4)$$

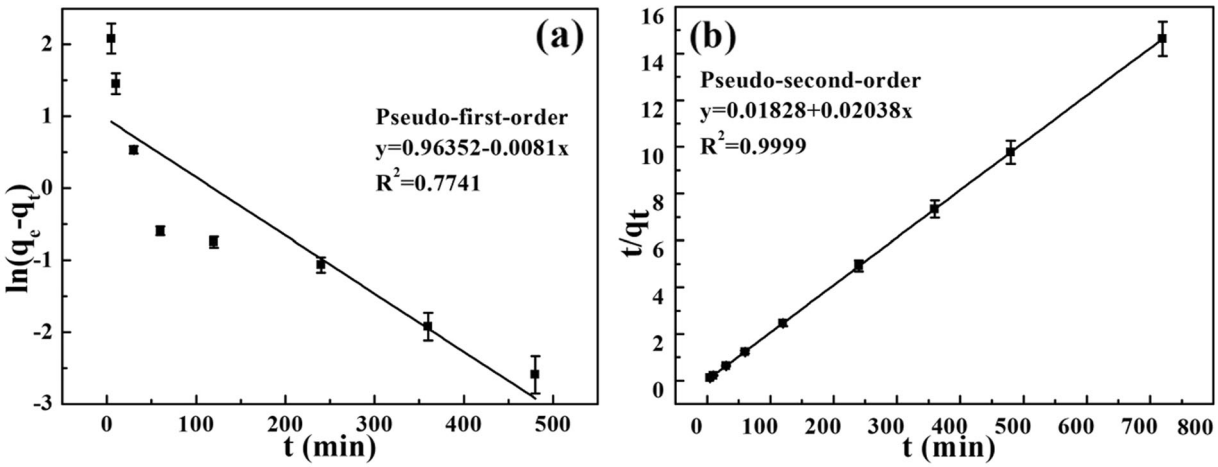

Fig. 8 The kinetic models of Hg(II) adsorption on PA-SNPs

Table 1 Kinetics parameters for mercury ions adsorption on PA-SNPs

Kinetics model	Parameters	Values
Pseudo-first-order kinetic	k_1 (min^{-1})	0.0081
	R^2	0.7741
Pseudo-second-order kinetic	k_2 (g/ mg·min)	0.0227
	R^2	0.9999

Where, q_e and q_t were the adsorption capacity (mg/g) at equilibrium time and at time t (min), respectively. k_1 and k_2 referred to the pseudo-first-order rate constant (min^{-1}) and pseudo-second-order rate constant (g/mg/min), respectively.

The experimental data of adsorption was fitted by linear plot of pseudo-first-order and pseudo-second-order models as $ln(q_e-q_t)$ vs. t and t/q_t vs. t, respectively. Figure 8 has given the results of the two models. The correlation coefficients (R^2) and kinetic parameters were listed in the Table 1. The pseudo-second-order model showed good fit for the adsorption of mercury on PA-SNPs. Because the correlation coefficient (R^2) of pseudo-second order model (0.9999) was much higher than that of the pseudo-first order model (0.7741). The pseudo-second-order model assumed that the rate determining step was chemisorption. This suggested that the adsorption of mercury ions on PA-SNPs was mainly the chemical reactive adsorption [35].

3.2.3 Effect of initial concentration on Hg(II) adsorption and adsorption isotherms

Figure 9 presented the relationship between adsorption capacity and the initial Hg(II) concentration. The adsorption capacity increased before the concentration of 600 mg/L and then attained a platform with the increase of mercury ions concentration. At low mercury ions concentration (<600 mg/L), there are enough functional groups and active

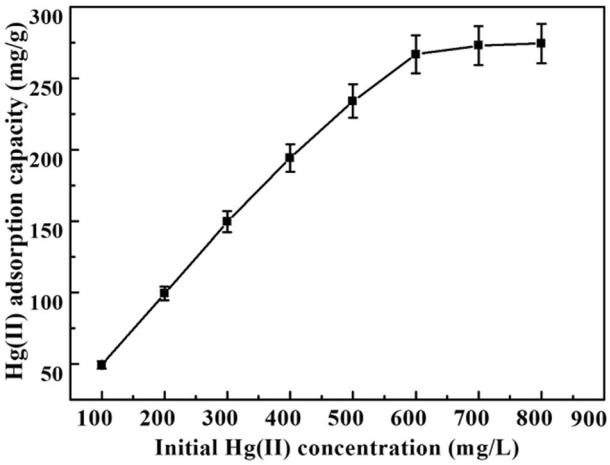

Fig. 9 Effect of initial concentration on Hg(II) adsorption

sites on the surface of PA-SNPs. The interaction between the metal ions and active sites can generate a potent driving force to defeat the resistances of the mercury ions mass transfer between the bulk solution and adsorbent [36]. So, the adsorption capacity increased with the increase of the mercury ions concentration. The maximum absorbability of mercury ions on PA-SNPs is 274.32 mg/g at the adsorption equilibrium.

In this study, Langmuir and Freundlich isotherm models were employed to describe the interaction between mercury ion and PA-SNPs. The linear form of the Langmuir and Freundlich are expressed by Eq. (7) and Eq. (8), respectively [37, 38]:

$$\frac{C_e}{q_e} = \frac{1}{q_{max} K_L} + \frac{C_e}{q_{max}} \tag{7}$$

$$\ln q_e = \ln K_F + \frac{1}{n} \ln C_e \tag{8}$$

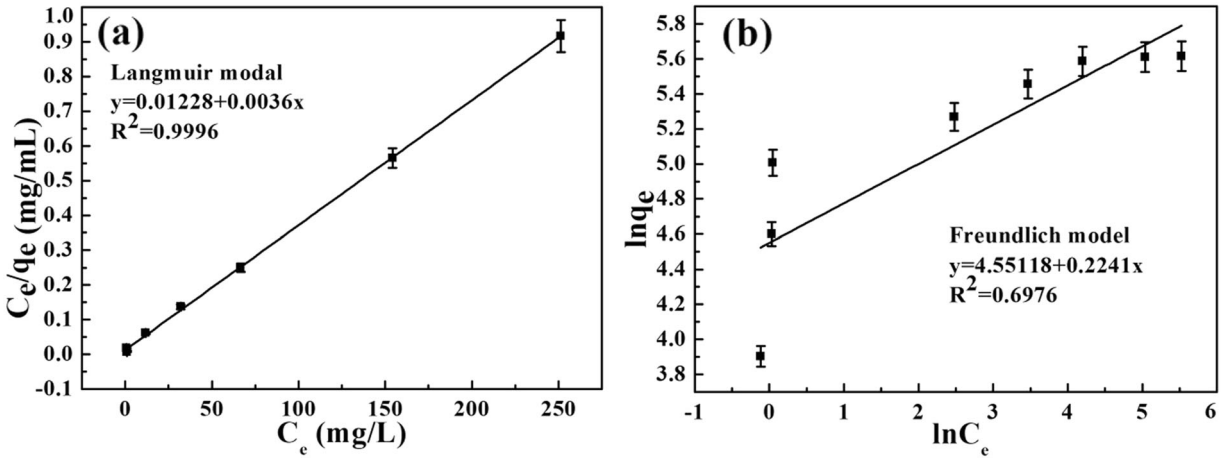

Fig. 10 The isotherm models of Hg(II) adsorption on PA-SNPs

Freundlich isotherm assumes that the adsorption sites with stronger affinity are first occupied and is applied to multilayer adsorption on heterogeneous surfaces with interactions between adsorbed molecules [39, 40] Langmuir isotherm assumes a monolayer adsorption on a homogenous surface where the binding sites have the same adsorption affinity and no interactions between adsorbates are considered [41, 42].

The experimental data of adsorption was fitted by linear plot of Langmuir and Freundlich models as C_e/q_e vs. C_e and lnq_e vs. lnC_e, respectively. Figure 10 presented the fitting results of the two isotherm models. The correlation coefficients (R^2) and fitting model parameters of the two models have been listed in Table 2. The Langmuir model better described the mercury ion adsorption process on PA-SNPs because the correlation coefficient (R^2, 0.9996) of Langmuir model is higher than that of Freundlich model (0.6976). Simultaneously, the theoretical maximum adsorption capacity of Langmuir model (277.78 mg/g) was closer to the experimental value (274.32 mg/g). Therefore, Langmuir model was more suitable for the novel adsorbent. Table 3 compares the adsorption capacity of the present work with others adsorbents reported in the literature. It can be clearly seen that PA-SNPs has the highest adsorption capacity for mercury ions among the listed absorbents.

Table 2 Isotherm parameters of mercury (II) adsorption

Isotherms models	Langmuir			Freundlich		
Parameters	q_{max}	K_L	R^2	K_F	n	R^2
Values	277.78	0.2932	0.9996	94.744	4.4623	0.6976

Table 3 Comparison of adsorption capacity of GD-SNPs with other adsorbents reported in literature

Absorbent	q_{max} (mg/g)	Ref.
Rice husk ash	4	[53]
chelating resin Chelex—100	14.2	[54]
Brazilian pepper biochars	15.1–24.2	[55]
polypyrrole-chitosan (PPy/CTN) nanocomposite	40	[56]
2-mercaptobenzothiazole-derivatized mesoporous silica	48	[57]
Sulfurized activated carbon	58.9	[58]
Moss peat	81.97	[59]
Thiolated carbon nanotube	105.6	[60]
Thiol-derivatized single walled carbon nanotube	131	[61]
Fe_3O_4@SiO_2–SH	132	[62]
Sulfur incorporated MWCNT	151.5	[63]
Polyrhodanine-encapsulated magnetic nanoparticles	179	[64]
Sulfamine modified chloromethylated polystyrene	222.2	[65]
PA-SNPs	274.32	This work

3.2.4 Selectivity

Selectivity is an indispensable factor in evaluating the adsorption properties of the absorbent. In our work, the selectivity of PA-SNPs was investigated in existing four coexisting ions (Zn(II), Ni(II), Mn(II) and Ge(IIII))[32, 43]. 20 mg of PA-SNPs was immersed into 10 mL of the mixed-ion solution (Hg(II), Zn(II), Ni(II), Mn(II), and Ge(IIII)) at pH 2.0. The initial concentration of all ions was 100 mg/L. The mixed-ion solution was vibrated for 6 h. Figure 11 has given the results of the selective adsorption of Hg(II) on PA-SNPs. The removal rate of mercury ions reached 98.94%, which is remarkably higher than that of the coexisting metal ions. Therefore, the mercury ion could be

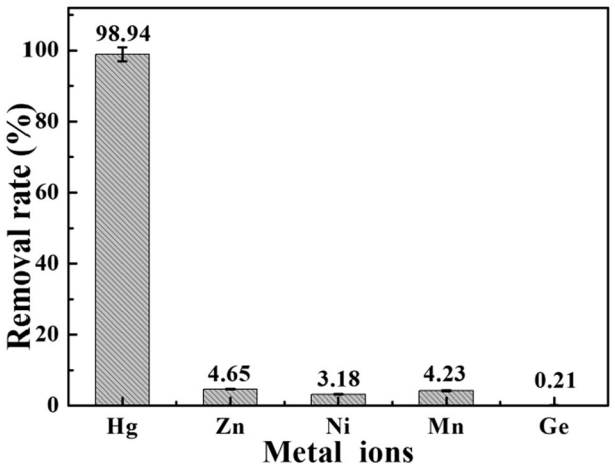

Fig. 11 Selective adsorption of Hg(II) on PA-SNPs

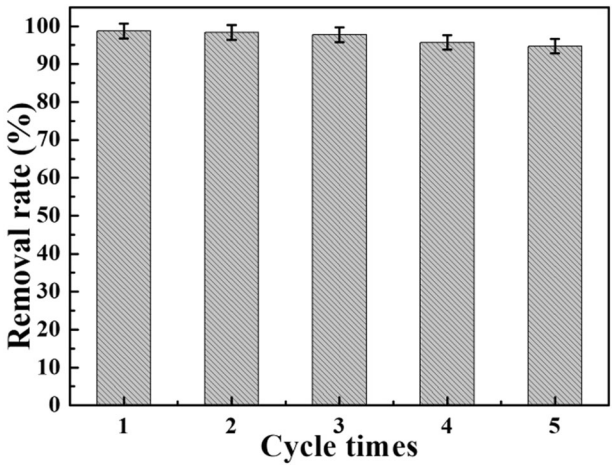

Fig. 12 Reusability of Hg(II) adsorption on PA-SNPs

selectively separated from the mixed metal ions solution by PA-SNPs. The high selectivity for mercury ions was resulted from the phosphonic acid groups of PA-SNPs. According to the theory of hard and soft acids-base [44, 45], the mercury ions was the soft nature metal ion and P atoms of PA-SNPs was soft bases which have a superior affinity with mercury ions. Therefore, mercury ions can be easily adsorbed by PA-SNPs and high selectivity was obtained.

3.2.5 Cyclic utilization and desorption experiments

To reduce the cost of removal process during practical application, it is very important to examine the desorption of Hg(II) from TPA-SNPs and regeneration of the spent adsorbent. Figure 12 has given the removal rate in each cycle. The adsorbent still remained good adsorption efficiency. The removal rate of mercury ions decreased slightly from 96.29 to 94.01%. The decrease might be caused by the loss of absorbent or irreversible occupation of part

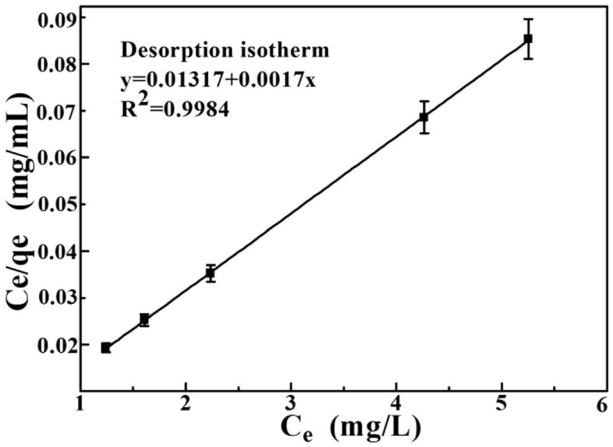

Fig. 13 Linearized Langmuir plots (C_e/q_e Vs. C_e) for desorption of PA-SNPs (desorbing agent of nitric acid (3 mol/L) and thiourea (1.5 mol/L))

adsorption sites [31]. So, PA-SNPs shows good reusability for the mercury recovery from aqueous solution.

Figure 13 has shown the desorption isotherm of PA-SNPs. Compared with Fig. 10a, the y-intercept values of the linearized Langmuir model of adsorption and desorption were the same. It is proved that mercury ions competed with the desorbing agent on the active adsorption sites [46]. Under the condition of nitric acid (3 mol/L), the surface of PA-SNPs is protonated, leading to the desorption of positively mercury ions [47]. The stable complexes and the electrostatic interactions between the charged thiourea species and mercury ions would weaken the interaction between the PA-SNPs and mercury ions and promoted desorption[48].

3.2.6 Adsorption mechanism

Based on some similar works, six adsorption mechanisms of mercury ions adsorption might be supposed (electrostatic interaction, ion exchange, ion-dipole interactions, coordination by surface metal cations, hydrogen bonding, and hydrophobic interaction) [49, 50]. In order to better understand the adsorption mechanism of mercury ions on the surface of PA-SNPs. The IR and XPS analysis were carried out in this study.

We defined Hg^{2+} loaded PA-SNPs as PA-SNPs-Hg. Figure 14 showed the FT-IR spectra of PA-SNPs and PA-SNPs-Hg. Compared with PA-SNPs, PA-SNPs-Hg presented a strong absorption peak at 1245 cm^{-1}, due to that the bonds of P=O and P-OH in phosphonic acid groups interacted with Hg^{2+}. This demonstrated that mercury ion was adsorbed through the chelating binding between Hg^{2+} and phosphorus groups on the surface of PA-SNPs.

To further verify the obtained results of adsorption mechanism from IR analysis, XPS analysis was carried

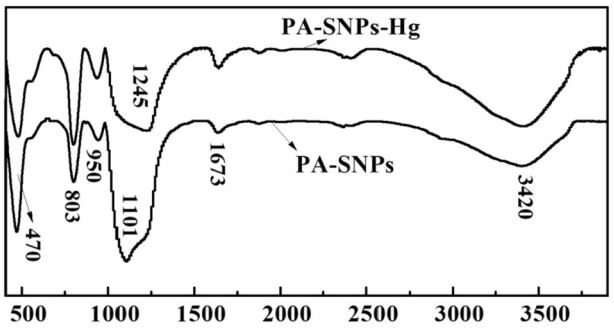

Fig. 14 FT-IR spectra of PA-SNPs and PA-SNPs-Hg

out to elucidate the adsorption mechanism. Figure 15a showed the wide-scan spectrum of PA-SNPs and PA-SNPs-Hg. Compared to the spectra of PA-SNPs, it can be clearly see that the Hg4f and Hg4d were appeared in PA-SNPs-Hg, suggesting the mercury ions were adsorbed by PA-SNPs. The peaks at 358.3 and 377.8 eV were attributed to Hg4d5 and Hg4d3, respectively (Fig. 15 b). The peaks at 100.7 and 103.9 eV in Fig. 15c were attributed to Hg-P bond and Hg4f5, respectively. The XPS analyses of mercury indicated that there existed stronger electron transfer between the adsorbed Hg^{2+} and PA-SNPs. So,

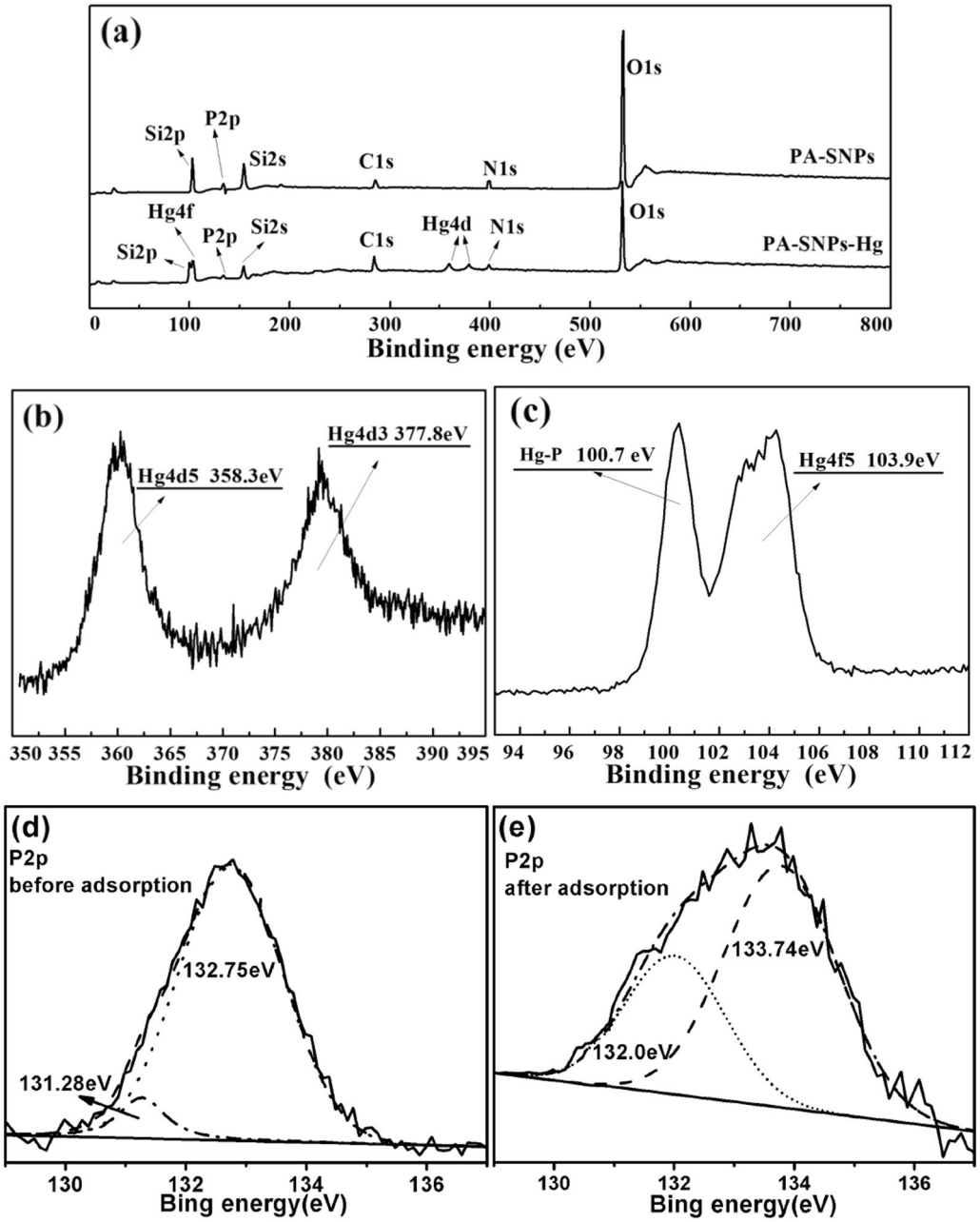

Fig. 15 XPS analyses of PA-SNPs and PA-SNPs-Hg **a**, XPS analyses of mercury **b**, **c** and P2p analyses **d**, **e**

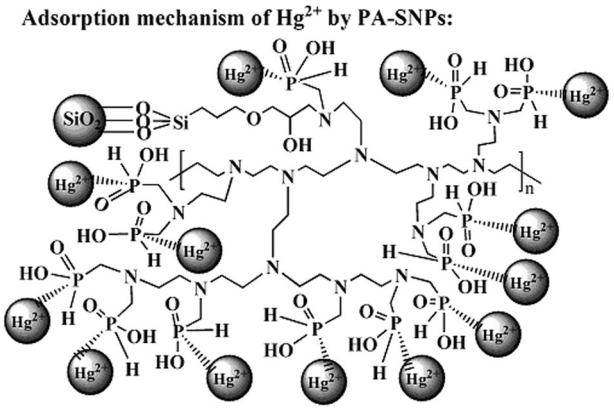

Scheme 2 Adsorption mechanism of mercury ions by PA-SNPs

the phosphorus atom groups on the surface of PA-SNPs play an important role in the adsorption process of mercury ion.

The P2p spectra of PA-SNPs and PA-SNPs-Hg were showed in Figs. 15d, e. The P2p spectra of PA-SNPs can be split into two peaks (131.28 and 132.75 eV), which correspond to P-C and P-O/P=O, respectively [51]. After adsorbed mercury ion, the two peaks were shifted to 132.0 and 133.74 eV. Because the mercury ions interacted with the P=O/P-OH groups on the surface of PA-SNPs [52]. Besides, Hg^{2+} shared the lone pairs of electrons from P atoms, resulting in the higher binding energies [19]. Therefore, chelation interaction was main mechanisms for the adsorption of mercury ions on the surface of PA-SNPs. The possible mechanism was presented in Scheme 2.

4 Conclusions

In this work, a novel adsorbent was prepared by modifying silica nanoparticles with phosphinic acid for mercury removal from aqueous solutions. The prepared adsorbent was characterized by TEM, FT-IR, TGA, and XPS. The adsorption properties of the adsorbent for mercury ions were investigated by batch adsorption experiments. Results showed that the optimum pH and the maximum adsorption capacity were 2.0 and 217.17 mg/g, respectively. PA-SNPs presented excellent selectivity for mercury ions among Zn (II), Ni(II), Mn(II), and Ge(IIII). Meanwhile, the reusability experiment showed that the novel adsorbent can be reused at least five times for the recovery of mercury ion. Besides, the adsorption process of mercury ions via PA-SNPs followed better with the pseudo-second-order kinetic model, which indicated that the interaction between Hg^{2+} and active groups on the PA-SNPs was chemical adsorption. Moreover, the equilibrium data fitted the Langmuir isotherm model very well, with a monolayer adsorption capacity of 277.78 mg/g. The main adsorption mechanism of mercury ion on PA-SNPs was chelation interaction between Hg^{2+} and PA-SNPs. Therefore, the novel nanosilica adsorbent has a potential application in the field of recovery of mercury ion from aqueous solution.

Acknowledgements The authors are grateful to the National Natural Science Foundation of China Project No: (51522405 and 51664037).

Funding This study was by National Natural Science Foundation of China Project No: (51522405 and 51664037).

Compliance with ethical standards

Conflict of interest The authors declare that they have no conflict of interest.

Informed consent All the authors agreed to submit to Journal of Sol–Gel Science and Technology

References

1. Yong J, Fang Y, Chen F, Huo J, Yang Q, Bian H, Du G, Hou X (2016) Femtosecondlaser ablated durable superhydrophobic PTFE films with micro-through-holesfor oil/water separation: separating oil from water and corrosive solutions. Appl Surf Sci 389:1148–1155
2. Gao CR, Sun ZX, Li K, Chen YN, Cao YZ, Zhang SY, Feng L (2013) Integrated oilseparation and water purification by a double-layer TiO_2-based mesh. Energy Environ Sci 6(4):1147–1151
3. Rocha CG, Zaia DA, Alfaya RV, Alfaya AA (2009) Use of rice straw as biosorbent for removal of Cu(II), Zn(II), Cd(II) and Hg (II) ions in industrial effluents. J Hazard Mater 166(1):383–388
4. Ariya PA, Amyot M, Dastoor A, Deeds D, Feinberg A, Kos G, Poulain A, Ryjkov A, Semeniuk K, Subir M, Toyota K (2015) Mercury physicochemical and biogeochemical transformation in the atmosphere and at atmospheric interfaces: a review and future directions. Chem Rev 11(10):3760–3802
5. Kabiri S, Tran DN, Azari S, Losic D (2015) Graphene-diatom silica aerogels for efficient removal of mercury ions from water. Acs Appl Mater Interfaces 7(22):11815–11823
6. Xiong YY, Li JQ, Gong LL, Feng XF, Meng LN, Zhang L, Meng PP, Luo MB, Luo F (2017) Using MOF-74 for Hg^{2+} removal from ultra-low concentration aqueous solution. J Solid State Chem 246:16–22
7. Rajamohan N, Rajasimman M, Dilipkumar M (2014) Parametric and kinetic studies on biosorption of mercury using modified Phoenix dactylifera biomass. J Taiwan Inst Chem Eng 45 (5):2622–2627
8. Ma X, Li Y, Ye Z, Yang L, Zhou L, Wang L (2011) Novel chelating resin with cyanoguanidine group: useful recyclable materials for Hg(II) removal in aqueous environment. J Hazard Mater 185(2-3):1348–1354
9. Shandil Y, Dautoo UK, Chauhan GS (2017) Mercury removal from aqueous solution using coke-derived sulfur-impregnated activated carbons. Chem Eng J 316:978–987
10. Yu Z, Dang Q, Liu C, Cha D, Zhang H, Zhu W, Zhang Q, Fan B (2017) Preparation and characterization of poly(maleic acid)-grafted cross-linked chitosan microspheres for Cd(II) adsorption. Carbohydr Polym 172:28–39
11. Ke F, Qiu LG, Yuan YP, Peng FM, Jiang X, Xie AJ, Shen YH, Zhu JF (2011) Thiol-functionalization of metal-organic framework by a facile coordination-based postsynthetic strategy and

enhanced removal of Hg^{2+} from water. J Hazard Mater 196 (12):36–43
12. Johari K, Saman N, Song ST, Chin CS, Kong H, Mat H (2016) Adsorption enhancement of elemental mercury by various surface modified coconut husk as eco-friendly low-cost adsorbents. Int Biodeterior Biodegrad 109:45–52
13. Songa ST, Haua YF, Samana N, Joharib K, Cheua SC, Konga H, Mat H (2016) Process analysis of mercury adsorption onto chemically modified rice straw in a fixed-bed adsorber. J Environ Chem Eng 4(2):1685–1697
14. Mudasir M, Karelius K, Aprilita NH, Wahyuni ET (2016) Adsorption of mecury(II) on dithizone-immobilized natural zeolite. J Environ Chem Eng 4(2):1839–1849
15. Deb AKS, Dwivedi V, Dasgupta K, Ali SM, Shenoy KT (2016) Novel amidoaminefunctionalized multi-walled carbon nanotubes for removal of mercury(II) ionsfrom wastewater: combined experimental and density functional theoreticalapproach. Chem Eng J 2016 313:899–911
16. Bao S, Li K, Ning P, Peng J, Jin X, Tang L (2017) Highly effective removal of mercury and lead ions from wastewater by mercaptoamine-functionalised silica-coated magnetic nano-adsorbents: Behaviours and mechanisms. Appl Surf Sci 393:457–466
17. Bo YS, Eom Y, Tai GL (2011) Removal and recovery of mercury from aqueous solution using magnetic silica nanocomposites. Appl Surf Sci 257(10):4754–4759
18. Mahmoud ME (2011) Surface loaded 1-methyl-3-ethylimidazolium bis(trifluoromethylsulfonyl)imide [EMIM $^{+}Tf^{2}N^{-}$], hydrophobic ionic liquid on nano-silica sorbents for removal of lead from water samples. Desalination 266(1-3):119–127
19. Xu G, Zhao Y, Hou L, Cao J, Tao M, Zhang W (2017) A recyclable phosphinic acid functionalized polyacrylonitrile fiber for selective and efficient removal of $Hg2^{+}$. Chem Eng J 325:533–543
20. Huang X, Dong J, Wang L, Feng Z, Xue Q, Meng X (2017) Selective recovery of rare earth elements from ion-adsorption rare earth element ores by stepwise extraction with HEH(EHP) and HDEHP. Green Chem 19(5):1345–1352
21. Liu P, Borrell PF, Božič M, Kokol V, Oksman K, Mathewa AP (2015) Nanocelluloses and their phosphorylated derivatives for selective adsorption of Ag^{+}, Cu^{2+}, and Fe^{3+} from industrial effluents. J Hazard Mater 294:177–185
22. Mautner A, Maples HA, Kobkeatthawin T, Kokol V, Karim Z, Li K, Bismarck A (2016) Phosphorylated nanocellulose papers for copper adsorption from aqueous solutions. Int J Environ Sci Technol 13(8):1861–1872
23. Xiong C, Wang S, Zhang L, Li Y, Zhou Y, Peng J (2018) Preparation of 2-aminothiazole-functionalized poly(glycidyl methacrylate) microspheres and their excellent gold ion adsorption properties. Polymers 10(5):159
24. Ram B, Chauhan GS (2018) New spherical nanocellulose and thiol-based adsorbent for rapid and selective removal of mercuric ions. Chem Eng J 331:587–596
25. Fan HT, Liu JX, Yao H, Zhang ZG, Yan F, Li WX (2014) Ionic imprinted silica-supported hybrid sorbent with an anchored chelating schiff base for selective removal of cadmium(II) ions from aqueous media. Ind Eng Chem Res 53(1):369–378
26. Tian B, Liu X, Yu C, Gao F, Luo Q, Xie S, Tu B, Zhao D (2002) Microwave assisted template removal of siliceous porous materials. Chem Commun 11(11):1186–1187
27. Tian Y, Yin P, Qu R, Wang C, Zheng H, Yu Z (2010) Removal of transition metal ions from aqueous solutions by adsorption using a novel hybrid material silica gel chemically modified by triethylenetetraminomethylenephosphonic acid. Chem Eng J 162 (2):573–579
28. Schlipf DM, Zhou S, Khan MA, Rankin SE, Knutson BL (2017) Effects of pore size and tethering on the diffusivity of lipids confined in mesoporous silica. Adv Mater Interfaces 4(9):1601103
29. Zhang L, Zhang G, Wang S, Peng J, Cui W (2017) Sulfoethyl functionalized silica nanoparticle as an adsorbent to selectively adsorb silver ions from aqueous solutions. J Taiwan Inst Chem Eng 71:330–337
30. Wang H, Zheng L, Liu G, Zhou Y (2018) Enhanced adsorption of Ag^{+} on triethanolamine modified titanate nanotubes. Colloids Surf A 537:28–35
31. Mauter MS, Elimelech M (2008) Environmental applications of carbon-based nanomaterials. Environ Sci Technol 42 (16):5843–5859
32. Wang Y, Zhang Y, Hou C, He X, Liu M (2015) Preparation of a novel TETA functionalized magnetic PGMA nano-absorbent by ATRP method and used for highly effective adsorption of Hg(II). J Taiwan Inst Chem Eng 58:283–289
33. Xiong C, Wang S, Zhang L, Li Y, Zhou Y, Peng J (2018) Selective recovery of silver from aqueous solutions by poly (glycidyl methacrylate) microsphere modified with trithiocyanuric acid. J Mol Liq 254:340–348
34. Plazinski W, Rudzinski W, Plazinska A (2009) Theoretical models of sorption kinetics including a surface reaction mechanism: a review. Adv Colloid Interface Sci 152(1-2):2–13
35. Repo E, Warchol JK, Kurniawan TA, Sillanpää MET (2010) Adsorption of Co(II) and Ni(II) by EDTA- and/or DTPA-modified chitosan: kinetic and equilibrium modeling. Chem Eng J 161(1-2):73–82
36. Arshadi M, Mousavinia F, Khalafinezhad A, Firouzabadi H, Abbaspourrad A (2017) Adsorption of mercury ions from wastewater by a hyperbranched and multi-functionalized dendrimer modified mixed-oxides nanoparticles. J Colloid Interface Sci 505:293–306
37. Xiong C, Li Y, Wang S, Zhou Y (2018) Functionalization of nanosilica via guanidinium ionic liquid for the recovery of gold ions from aqueous solutions. J Mol Liq 256:183–190
38. Attari M, Bukhari SS, Kazemian H, Rohani S (2016) A Low-cost adsorbent from coal fly ash for mercury removal from industrial wastewater. J Environ Chem Eng 5(1):391–399
39. Wawrzkiewicz M (2010) Application of weak base anion exchanger in sorption of tartrazine from aqueous medium. Solvent Extr Ion Exch 28(6):845–863
40. Fu J, Chen Z, Wang M, Liu S, Zhang J, Zhang J, Han R, Xu Q (2015) Adsorption of methylene blue by a high-efficiency adsorbent (polydopamine microspheres): kinetics, isotherm, thermodynamics and mechanism analysis. Chem Eng J 259:53–61
41. Ho YS, Porter JF, Mckay G (2002) Equilibrium isotherm studies for the sorption of divalent metal ions onto peat: copper, nickel and lead single component systems. Water Air Soil Pollut 141(1-4):1–33
42. Dong Z, Liu J, Yuan W, Yi Y, Zhao L (2016) Recovery of Au(III) by radiation synthesized aminomethyl pyridine functionalized adsorbents based on cellulose. Chem Eng J 283:504–513
43. Awual MR (2016) Novel nanocomposite materials for efficient and selective mercury ions capturing from wastewater. Chem Eng J 307:456–465
44. Xiong C, Li Y, Wang G, Fang L, Zhou S, Yao C, Chen Q, Zheng X, Qi D, Fu Y, Zhu Y (2015) Selective removal of Hg(II) with polyacrylonitrile-2-amino-1,3,4-thiadiazole chelating resin: batch and column study. Chem Eng J 259:257–265
45. Wang Z, Yin P, Wang Z, Qu R, Liu X (2012) Chelating resins silica gel supported aminophosphonic acids prepared by a heterogeneous synthesis method and a homogeneous synthesis method and the removal properties for Hg (II) from aqueous solutions. Ind Eng Chem Res 51(25):8598–8607

46. Khan MA, Wallace WT, Islam SZ, Nagpure S, Strzalka J, Littleton JM, Rankin SE, Knutson BL (2017) Adsorption and recovery of polyphenolic flavonoids using TiO2 functionalized mesoporous silica nanoparticles. Acs Appl Mater Interfaces 9 (37):32114–32125
47. Bogusz A, Oleszczuk P, Dobrowolski R (2015) Application of laboratory prepared and commercially available biochars to adsorption of cadmium, copper and zinc ions from water[J]. Bioresour Technol 196:540–549
48. Fujiwara K, Ramesh A, Maki T, Hasegawa H, Ueda K (2007) Adsorption of platinum (IV), palladium (II) and gold (III) from aqueous solutions onto l-lysine modified crosslinked chitosan resin. J Hazard Mater 146(1-2):39–50
49. Liu M, Hou LA, Xi B, Zhao Y, Xia X (2013) Synthesis, characterization, and mercury adsorption properties of hybrid mesoporous aluminosilicate sieve prepared with fly ash. Appl Surf Sci 273(100):706–716
50. Derylo-Marczewska A, Buczek B, Swiatkowski A (2011) Effect of oxygen surface groups on adsorption of benzene derivatives from aqueous solutions onto active carbon samples. Appl Surf Sci 257(22):9466–9472
51. Viornery C, Chevolot Y, Leonard D, Aronsson BO, Pechy P, Mathieu HJ, Descouts P, Graetzel M (2002) Surface modification of titanium with phosphonic acid to improve bone bonding: characterization by XPS and ToF-SIMS. Langmuir 18:2582–2589
52. Chen Y, Zhu B, Wu D, Wang Q, Yang Y, Ye W, Guo J (2012) Eu (III) adsorption using di(2-thylhexly) phosphoric acid-immobilized magnetic GMZ bentonite. Chem Eng J 181-182:387–396
53. El-Said AG, Badawy NA, Garamon SE (2010) Adsorption of cadmium (II) and mercury (II) onto natural adsorbent rice husk ash (RHA) from aqueous solutions: study in single and binary system. J Am Sci 6:400–409
54. Amara-Rekkab A, Didi MA (2014) Liquid–Solid extraction of mercury (II) from aque- ous solution by chelating resin Chelex-100. Eur Chem Bull 3:860–868
55. Dong X, Ma LQ, Zhu Y, Li Y, Gu B (2013) Mechanistic investigation of mercury sorption by brazilian pepper biochars of different pyrolytic temperatures based on X-ray photoelectron spectroscopy and flow calorimetry. Environ Sci Technol 47 (21):12156–12164
56. Salahi S, Ghorbani M (2014) Adsorption parameters studies for the removal of mercury from aqueous solutions using hybrid sorbent. Adv Polym Technol 33(4):1–6
57. Pérez-Quintanilla D, Del HI, Fajardo M, Sierra I (2006) Preparation of 2-mercaptobenzothiazole-derivatized mesoporous silica and removal of Hg(ii) from aqueous solution. J Environ Monit Jem 8(1):214–222
58. Asasian N, Kaghazchi T, Faramarzi A, Hakimi-Siboni A, Asadi-Kesheh R, Kavand M, Mohtashami S (2014) Enhanced mercury adsorption capacity by sulfurization of activated carbon with SO_2 in a bubbling fluidized bed reactor. J Taiwan Inst Chem Eng 45:1588–1596
59. Bulgariu L, Ratoi M, Bulgariu D, Macoveanu M (2008) Equilibrium study of Pb (II) and Hg (II) sorption from aqueous solutions by moss peat. Environ Eng Manag J 7(5):511–516
60. Hadavifar M, Bahramifar N, Younesi H, Li Q (2014) Adsorption of mercury ions from synthetic and real wastewater aqueous solution by functionalized multi-walled carbon nanotube with both amino and thiolated groups. Chem Eng J 237(2):217–228
61. Bandaru NM, Reta N, Dalal H, Ellis AV, Shapter J, Voelcker NH (2013) Enhanced adsorption of mercury ions on thiol derivatized single wall carbon nanotubes. J Hazard Mater 261:534–541
62. Wang Z, Xu J, Hu Y, Zhao H, Zhou J, Liu Y, Lou Z, Xu X (2016) Functional nanomaterials: Study on aqueous Hg(II) adsorption by magnetic Fe_3O_4@SiO_2-SH nanoparticles. J Taiwan Inst Chem Eng 60:394–402
63. Gupta A, Vidyarthi SR (2014) Sankararamakrishnan N. Enhanced sorption of mercury from compact fluorescent bulbs and contaminated water streams using functionalized multiwalled carbon nanotubes. J Hazard Mater 274(12):132–144
64. Song J, Kong H, Jang J (2011) Adsorption of heavy metal ions from aqueous solution by polyrhodanine-encapsulated magnetic nanoparticles. J Colloid Interface Sci 359(2):505–511
65. Qi Y, Jin X, Yu C, Wang Y, Yang L, Li Y (2013) A novel chelating resin containing high levels of sulfamine group: preparation and its adsorption characteristics towards p-toluenesulfonic acid and Hg(II). Chem Eng J 233(11):315–322